17315 (1992).
15. Semm, P. & Beason, R. C. Responses to small magnetic field variations by the trigeminal system of the bobolink. *Brain Res. Bull.* **25,** 735–740 (1990).
16. Walker, M. M. Learned magnetic field discrimination in the yellowfin tuna, *Thunnus albacares*. *J. Comp. Physiol. A* **155,** 673–679 (1984).
17. Walker, M. M. & Bitterman, M. E. Honeybees can be trained to respond to very small changes in geomagnetic field intensity. *J. Exp. Biol.* **145,** 489–494 (1989).
18. Wiltschko, R. & Wiltschko, W. *Magnetic Orientation in Animals.* (Springer, Berlin, Heidelberg, New York, 1995).
19. Gould, J. L., Kirschvink, J. L., Deffeyes, K. S. Bees have magnetic remanence. *Science* **201,** 1026–1028 (1978).
20. Lohmann, K. J. Magnetic remanence in the Western Atlantic spiny lobster. *J. Exp. Biol.* **113,** 29–41 (1984).
21. Walker, M. M. On a wing and a vector: A model for magnetic navigation by homing pigeons. *J. Theor. Biol.* **192,** 341–349 (1998).
22. Walker, M. M. Magnetic position determination by homing pigeons. *J. Theor. Biol.* **197,** 271–276 (1999).
23. Proksch, R. B., Runge, E., Hansma, P. K., Foss, S. & Walsh, B. High field magnetic force microscopy. *J. Appl. Phys.* **78,** 3303–3307 (1995).
24. Liou, S. H. & Yao, Y. D. Development of high coercivity magnetic force microscopy tips. *J. Magn. Magn. Mater.* **190,** 130–134 (1998).

Acknowledgements

We thank K. Babcock at Digital Imaging for the generous use of the AFM/MFM. The Biological Imaging Research Unit at the School of Medicine, University of Auckland, provided the CLSM and imaging facilities. In addition, we thank S. Edgar, A. Turner, H. Holloway and especially B. Beaumont for their assistance in preparation and viewing samples on the CLSM and transmission electron microscopy. Financial support came from the Marsden Fund and the School of Biological Sciences.

Correspondence and requests for materials should be addressed to C.E.D. (e-mail: cdiebel@akmuseum.org.nz) or M.M.W. (e-mail: m.walker@auckland.ac.nz).

Transformation from temporal to rate coding in a somatosensory thalamocortical pathway

Ehud Ahissar, Ronen Sosnik & Sebastian Haidarliu

Department of Neurobiology, The Weizmann Institute of Science, Rehovot 76100, Israel

The anatomical connections from the whiskers to the rodent somatosensory (barrel) cortex form two parallel (lemniscal and paralemniscal) pathways[1,2]. It is unclear whether the paralemniscal pathway is directly involved in tactile processing, because paralemniscal neuronal responses show poor spatial resolution, labile latencies and strong dependence on cortical feedback[3–5]. Here we show that the paralemniscal system can transform temporally encoded vibrissal information into a rate code. We recorded the representations of the frequency of whisker movement along the two pathways in anaesthetized rats. In response to varying stimulus frequencies, the lemniscal neurons exhibited amplitude modulations and constant latencies. In contrast, paralemniscal neurons in both thalamus and cortex coded the input frequency as changes in latency. Because the onset latencies increased and the offset latencies remained constant, the latency increments were translated into a rate code: increasing onset latencies led to lower spike counts. A thalamocortical loop that includes cortical oscillations and thalamic gating can account for these results. Thus, variable latencies and effective cortical feedback in the paralemniscal system can serve the processing of temporal sensory cues, such as those that encode object location during whisking. In contrast, fixed time locking in the lemniscal system is crucial for reliable spatial processing.

The lemniscal pathway of the rat trigeminal system ascends through the ventral posterior medial nucleus (VPM) of the thalamus to the barrels in layer 4 of the cortex and to layers 5b and 6 (refs 6, 7). The paralemniscal pathway ascends through the medial division of the posterior nucleus (POm) of the thalamus to layers 1 and 5a and to the septa between the barrels in layer 4 (refs 7, 8). To reveal the processing differences between the two pathways, we recorded from single-units (n = 710) and multi-units (n = 540) of the major stations along these pathways while we stimulated (moved) the whiskers. First we analysed single- and multi-units separately. Analysis of the single-units revealed that response patterns were usually similar for neighbouring neurons. Therefore, spikes of all single- and multi-units that were recorded simultaneously from a single electrode were pooled, and these pools were referred to as 'local populations'.

First, we examined responses to stimuli that mimic natural whisking conditions[9]: 50-ms pulses of air puffs applied to one or two rows of whiskers at 8 Hz. Typical recordings along both pathways are shown in Fig. 1. Brainstem neurons appeared simply to

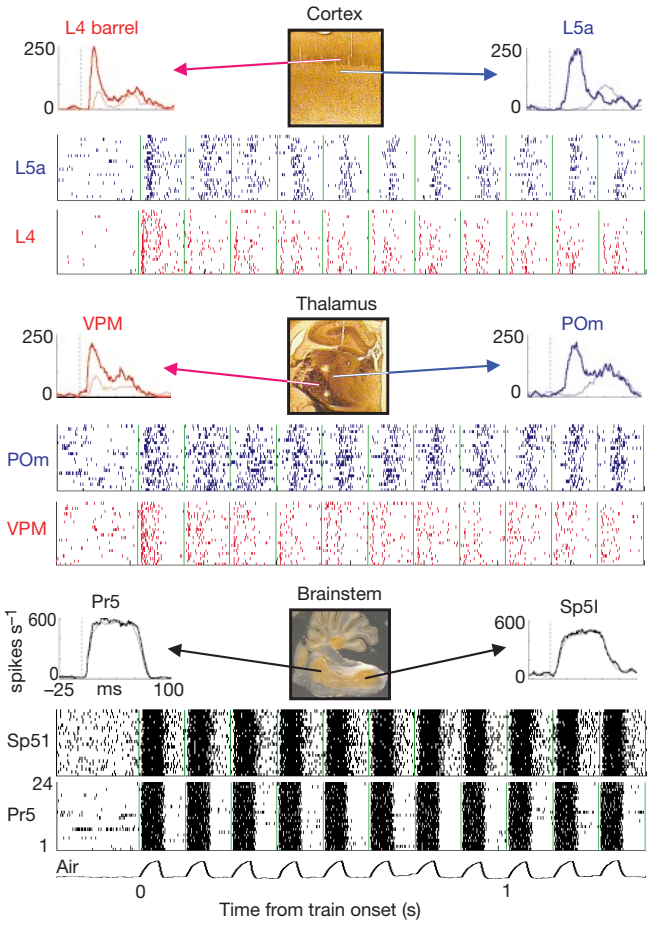

Figure 1 Lemniscal and paralemniscal thalamic transformations. Recordings of local populations from the six major stations along both pathways. Raster displays show firing times of recorded neurons (black, red or blue vertical lines) in relation to stimulus onset times (green vertical lines). Responses to 24 stimulus trains are plotted. PSTHs were computed for each stimulus cycle and are shown for the first (at time 0; thick curves) and last three cycles of the figure (cycles 9–11; thin curves). Response patterns remained steady during the remaining 13 cycles (not shown). The main trigeminal nuclei (Pr5 and Sp5I) receive vibrissal input and project to both thalamic nuclei, with a bias of Pr5 towards VPM and Sp5I towards POm[16,29]. VPM projects to cortical barrels (dark areas in layer 4) and layers 5b and 6, and receives feedback from the upper part of layer 6 (refs 6, 7, 30). POm projects to layers 1 and 5a, and the septa between the barrels in layer 4 (refs 7, 8), and receives feedback from layer 5 and the lower part of layer 6 (refs 7, 30). Electrolytic lesions in the thalamus mark recording locations of single local populations in the POm (upper) and VPM.

relay primary afferent responses[10]: the response to a single pulse was constant along the train, as evident from the raster display and from the overlap between the peristimulus time histograms (PSTHs) computed for the first cycle (thick lines) and for the last three cycles (thin lines). However, as expected[4,11], thalamic neurons did not behave as relays, and their outputs exhibited specific transformations of the brainstem signals (Fig. 1, middle rows). The transformation at the VPM resembled an adaptation process during which, following the first stimulation cycle, the spike count (per stimulus cycle) decreased as the train continued, until a 'steady state' (a period during which the spike count was steady) was reached. Recordings from the POm revealed a different stabilization process. The latency of the response onset increased during the 8-Hz train until it stabilized at a significantly longer steady-state value (Fig. 1, POm raster display and PSTHs). These latency shifts resulted in decreased spike counts in the POm neurons because offset latencies did not change. In the barrel cortex there was a similar dissociation for the response patterns of the lemniscal and paralemniscal projection targets (Fig. 1, top rows). Whereas the responses of layer 4 barrel neurons were similar to those of VPM neurons, the responses of layer 5a neurons resembled those of POm neurons. These response patterns were so characteristic for single- and multi-units at each station that the recording location could often be predicted based on the physiological responses, even before histological processing.

Next, we tested the dependency of the thalamic transformations on the frequency of whisker movement using three frequencies (2, 5 and 8 Hz), revealing another dissociation between the two pathways. Whereas steady-state latencies of the lemniscal pathway were almost constant for all the tested frequencies, those of the paralemniscal pathway increased with increasing frequencies. The pathway-specific response patterns are demonstrated by the PSTHs that were averaged, for each station, across all neurons recorded from well localized sites (Fig. 2). At a stimulation frequency of 2 Hz (below the natural whisking range), latencies at all stations barely changed between the first stimulus cycles (left insets) and the steady-state periods (centre PSTHs). With stimulation frequencies of 5 and 8 Hz (both of which are within the whisking frequency range[12]), brainstem and lemniscal latencies were also essentially constant (Fig. 2, centre PSTHs and right insets), in agreement with other findings[10]. However, steady-state latencies of the paralemniscal pathway increased with increasing stimulus frequency (Fig. 2, centre PSTHs and right insets; see also ref. 3).

For both pathways, the magnitude of the steady-state responses (measured by the PSTH area, that is, spike counts per cycle) decreased with increasing frequencies. Again, in the lemniscal pathway, spike-count decrements were caused by amplitude reduction, whereas in the paralemniscal pathway they resulted primarily from latency shifts. As a result, during steady-state periods of whisker stimulation, whisker frequencies were represented by spike counts (rate coding) in both pathways, and by latencies (temporal coding) in the paralemniscal pathway. These representations were reproduced during each stimulus train, as the responses to the first cycle in each train were identical for all frequencies (Fig. 2, left insets). The averaged latency and spike-count representations of the whisker frequency (Fig. 2, right insets) depict typical representations of single local populations in each of the stations. These pathway-specific representations occurred for all well localized recording sites, except for 1 out of 14 in POm and 1 out of 13 in layer 5a, in both of which the latency increased between 2 and 5 Hz but not between 5 and 8 Hz. Part of the amplitude adaptation could be attributed to anaesthesia[10]. However, anaesthesia could not account for the latency shifts in the paralemniscal system, because latency shifts due to anaesthesia are an order of magnitude smaller[13–15]. Furthermore, as these latency shifts developed during each stimulus train, they probably reflect a dynamic process.

Paralemniscal processing could be conducted in parallel to, or in series with[2,4,5], lemniscal processing. If processing is in series, the onset of POm activity should lag the onset of lemniscal cortical activity. However, as seen in Fig. 3, which shows the average responses to the first cycle of mechanical stimulation applied to the principal whiskers, the average POm response rises before those of layers 4 and 5b. Furthermore, the shortest and modal latencies to the first stimulus cycle in the POm (7 and 8 ms, respectively) were shorter than those in layer 4 (8 and 9 ms) and layer 5b (8 and 9 ms). Thus, the onset of POm activity must be driven directly by the onset

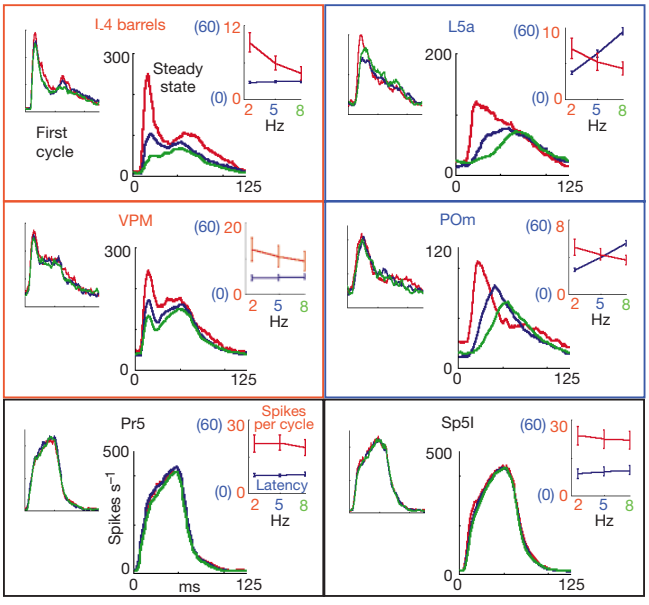

Figure 2 Response transformations and steady-state frequency representations. For each station, data was averaged across all well localized local populations (5, 5, 7, 14, 9 and 13 local populations from Pr5, Sp5I, VPM, POm, layer 4 barrels and layer 5a, respectively). Air puffs (50 ms) moved the whiskers anteriorly (protraction direction) at 2 (red), 5 (blue) and 8 Hz (green). For each station, the average PSTH for the first stimulus cycle (left) and steady-state period (0.5–3 s; middle; scales as for first stimulus cycle) are shown. On the right of each panel are the average (± s.e.m.) spike count (red) and latency (blue) as a function of stimulation frequency. These averages were computed across all well localized local populations of each station during steady states. Latencies to half peak are shown. A significant dependency of latency on frequency was found only in POm and layer 5a (POm, $r^2 = 0.62$, $P < 0.0001$; layer 5a, $r^2 = 0.71$, $P < 0.0001$; in all brainstem and lemniscal stations, slope < 0.5 ms Hz^{-1}, $r^2 < 0.03$ and $P > 0.44$).

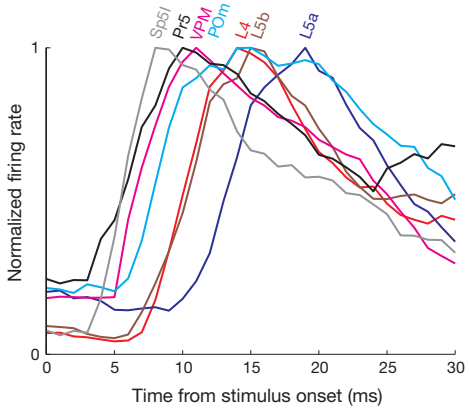

Figure 3 Order of activation onset. Average PSTHs of the entire population recorded at each station during the first cycle of a mechanical stimulus train applied to the principal whisker (forward deflections using the mechanical stimulator). Sp5I ($n = 14$ units), Pr5 ($n = 10$), VPM ($n = 12$), POm ($n = 17$), layer 4 barrels (L4; $n = 22$), layer 5b (L5b; $n = 24$) and layer 5a (L5a; $n = 26$).

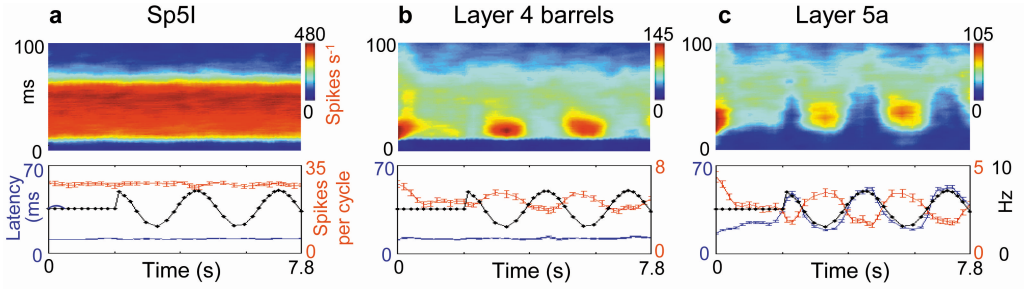

Figure 4 Representations of the instantaneous whisker frequency. **a**, An Sp5I local population. **b**,**c**, Pooled data from all well localized local populations of cortical layer 4 barrels ($n = 9$) and layer 5a ($n = 6$) recorded during FM stimulations. In each station, pooled data is represented by the population response composed of all spikes generated by the different units recorded from the same station in different subjects and at different times. Spike times were coordinated according to onset times of the stimulus trains. Top, PSTHs as a function of train time (vertical axis, PSTH time; horizontal, train time; colour axis, firing rate). Bottom, instantaneous stimulus frequencies (black), response latencies (blue) and spike counts (red) as a function of train time. Means of 36 trials ± s.e.m. Standard errors of the latency were computed; for each stimulus cycle, from the inter-trial variability of the latency to the first spike. Firing rates, spike counts and latencies were smoothed along train time by a convolution with a triangle of area 1 and base of ± 1 cycle.

of brainstem activity, which is transferred along the paralemniscal pathway in parallel with the activity conveyed along the lemniscal pathway. These results are consistent with the 1–2-ms delay between VPM and POm activation by brainstem electrical stimulations[16]. Of course, POm activity following the onset of activation could be affected by mixed lemniscal and paralemniscal cortical feedback. However, the similarity between the transient and steady-state response patterns within each pathway (Figs 1, 2) indicates that the sustained activation may also be pathway-specific, and that it is dominated, at least to a first approximation, by closed thalamocortical loops in each pathway.

A striking feature of the paralemniscal response pattern is that while the onset latency increased, the offset latency remained constant, which caused a reduction in the duration of the response and hence reduced spike counts. The latency increments cannot simply be attributed to VPM–POm interactions. These interactions are inhibitory[17], which predicts a positive correlation between the response strength of the VPM neurons and the latencies of the POm neurons, whereas we observed the opposite (Fig. 2). However, an alternative explanation, based on closed-loop operation of the paralemniscal thalamocortical system, is consistent with our results. This explanation suggests that thalamocortical circuits implement phase-locked loops, a computational algorithm that is optimal for temporal decoding[18,19].

An implementation of a POm–cortex phase-locked loop that is consistent with the findings presented here is based on a simple closed-loop thalamocortical circuit[20] that includes cortical inhibition[20,21], cortical oscillatory mechanisms[22–24] and thalamic gating[25]. Briefly, this circuit establishes a negative feedback loop in which the latency of the cortical oscillations determines the latency and spike count of the thalamic neurons, and the thalamic spike count determines the subsequent latency of the cortical oscillations. Within such a circuit, thalamic and cortical latencies do not depend directly on the brainstem latency, but rather on the latency of the cortical oscillations. Consistent with the model and results presented here, cortical oscillating neurons display increasing latencies with increasing stimulus frequencies[24] (see Supplementary Information for a more detailed description of the model).

When properly tuned, such a simple thalamocortical circuit should be able to track changes in the input frequency with a delay of a single cycle, and to represent these changes in the latencies and spike counts of its thalamic and cortical neurons[18] (see Supplementary Information). To achieve this, thalamic neurons must function in their gating mode. However, following a quiescent period, thalamic neurons shift to a non-gating mode in which their outputs do not appear to depend on the cortical signal[25]. This can account for the relatively short latency of POm neurons to the first stimulus cycle (Figs 1–3) and the relatively long period required for stabilization (Fig. 1). In the awake animal, thalamic neurons probably shift into a gating mode upon whisking[13].

We tested the performance of the POm–cortex circuits in single-cycle temporal decoding by applying frequency-modulated (FM) stimuli as follows. To shift the thalamic neurons into a gating mode and to allow 'locking in' of the thalamocortical circuits[18], the whisker stimulation frequency was first kept constant at 5 Hz for 2 s. Then the stimulus frequency was modulated for an additional 6 s (40% modulation depth, 0.4 Hz, initial phase 90°). The entire process was repeated 36 times for each simultaneous recording, and the responses of each local population were averaged across repetitions.

In the brainstem, the response to each stimulus cycle was the same, regardless of the instantaneous frequency (the reciprocal of the current period) of the stimulus (Fig. 4a). In contrast, once 'locked in' to the stimulus, paralemniscal thalamic and cortical neurons directly represented the input frequency, by both latency and spike-count, with almost no delay (see pooled layer 5a representation in Fig. 4c). The spike-count and latency representations were usually linearly related, reflecting the transformation of latency to spike count observed in this system. Linear regression estimates of spike counts from latencies could explain most of the spike count variability for layer 5a ($r^2 = 0.66 \pm 0.2$, $n = 6$, $P < 0.0001$) and POm ($r^2 = 0.51 \pm 0.12$, $n = 9$, $P < 0.0001$) local populations. As expected from the steady-state data, whisker frequency was represented by spike count alone in the lemniscal pathway (see pooled barrel representation in Fig. 4b). The lemniscal spike-count representation was not sensitive to the fast frequency transition (at $t = 2$ s) and exhibited a smaller dynamic range than the paralemniscal one (modulation depths of the spike-count representations were 12.5 ± 15% ($n = 13$) for VPM and layer 4 barrel neurons, and 25.5 ± 14.5% ($n = 15$) for POm and layer 5a neurons ($P < 0.05$, two-tailed t-test)). Thus, the temporal information of the stimulus was not reliably re-coded by lemniscal firing rates, even though the temporal information was faithfully replicated by lemniscal firing times.

During exploration and active touch, rats move their whiskers back and forth at frequencies between 4 and 11 Hz[9,12,13,19]. These whisking movements yield spatial and temporal encoding of the external spatial information. For example, object location (relative to the face and initial position of whiskers) is encoded by the identity of the activated whiskers (spatial encoding) and by the temporal interval between protraction onset and perturbation by the object (temporal encoding)[26]. Our results indicate that these two components may be processed separately and in parallel, in the lemniscal and paralemniscal pathways, respectively. The loss of time

locking to stimulus onset in the paralemniscal system is a reflection of the temporal-to-rate code translation process, in which latency shifts produce a rate-coded representation of the whisker frequency. The fixed time locking preserved along the lemniscal system probably reflects a lack of temporal processing within the whisking frequency range. On the other hand, the fixed time locking is required for reliable spatial processing during whisking, because, owing to whisker movements, temporal uncertainties in afferent firings result in uncertainties about whisker location. Thus, counterintuitively, fixed time locking is crucial for spatial processing, whereas variable latencies serve temporal processing. The response durations of the paralemniscal neurons are well tuned for temporal processing in the frequency range of whisking, as these response durations match the duration of a single protraction phase (>50 ms) and thus allow the decoding of all possible temporal intervals during protraction. Note that decoding of temporal information at higher frequencies, such as those that encode the texture of objects scanned by the whiskers[9], probably cannot be achieved by the slow paralemniscal system, but can be achieved by lemniscal thalamocortical circuits in which high frequencies can be coded (and translated to rate) by fine modulations of the response latency.

Our data indicate that the paralemniscal pathway of the rat somatosensory system is optimally tuned for temporal processing of vibrissal information around the whisking frequency range (~ 8 Hz), and that temporally encoded information can be translated to a rate code by thalamocortical loops. These findings point towards a parallel processing scheme in which spatially encoded (and perhaps high-frequency, temporally encoded) information is decoded by the lemniscal system, whereas low-frequency, temporally encoded information is decoded by the paralemniscal system. Sensory pathways dedicated to temporal processing have been reported in the electric fish and in the auditory brainstem of birds and mammals[27]. Here we provide evidence for a separate sensory pathway for temporal processing that involves the thalamus and cortex. □

Methods

Animal procedures and electrophysiology

Experimental procedures were similar to those used previously[24,28]. Briefly, 43 adult male Wistar albino rats (300 ± 25 g) obtained from the Animal Breeding Unit of The Weizmann Institute of Science were anaesthetized (urethane, 1.5 g kg^{-1}, injected intraperitoneally) and mounted in a modified stereotaxic device that allows free access to the somatosensory cortex and vibrissae. We monitored the depth of anaesthesia by assessing corneal and limb-withdrawal reflexes, and maintained it at stage III/3–4 (as determined by the dominant frequencies in the power spectra of local field potentials in the cortex[14]) by injections of urethane (10% of initial dose). Atropine methyl nitrate (0.3 mg kg^{-1}, intramuscular) was administered before general anaesthesia to prevent respiratory complications. Body temperature was maintained at ~ 37 °C.

The skull was exposed, and openings were made to allow electrode penetrations to different neuronal stations in the barrel cortex, thalamus and/or brainstem. Four to eight microelectrodes were driven into one or two stations simultaneously using one or two microdrive systems[28]. We isolated single units by spike templates and multiple units by amplitudes using spike sorters (MSD-2; Alpha-Omega). We recorded 96 single-units and 62 multi-units in the brainstem, 333 and 234, respectively, in the thalamus, and 281 and 244, respectively, in the cortex. The number of neurons recorded by a single electrode (a local population) was estimated to be 5 ± 1.3 (mean $\pm$ s.d.) neurons. The care and treatment of rats were in accordance with the animal welfare guidelines of The Weizmann Institute of Science.

Whisker stimulation

Whisker stimulations consisted of pulses of compressed air, generated by a pneumatic pressure pump (Medical Systems) and delivered through 3 m of stiff, thick-walled tubing (6.5 mm outer diameter, 3.5 mm inner diameter). A micropipettor tip was attached to the end of the tubing to reduce its opening to a diameter of 0.7 mm and was positioned 10–20 mm caudally to the most caudal whiskers of the stimulated rows. We usually stimulated one or two rows of whiskers (including at least the four most caudal whiskers and associated straddlers). Constant-frequency stimuli were applied in blocks of $12(\times 2)$ or 24 trains of 3 or 4 s each, with inter-train intervals of 2 or 1 s, respectively. FM stimuli were applied in blocks of 36 trains of 8 s each, with inter-train intervals of 2 s. The stimuli were delivered as constant pulses (see bottom trace in Fig. 1): during the first 50 ms of each cycle the whiskers were protracted (rise time, 30 ms; maximum pressure level at pump output, 0.7 kg cm^{-2}) and then allowed to retract (fall time, 10 ms). Pulse profiles were equal for all the frequencies used. Air-puff delays (from pump command to whisker movement) were calibrated using a microphone. In all experiments, latencies evoked by air puffs were compared with those evoked by a mechanical stimulator[28], which was attached to a single whisker 5–10 mm from the skin (amplitude, 560 μm; rise and fall times, 5 ms). When mismatches (all were <3 ms) were detected, the mechanical latencies were assumed.

Histology

We analysed the brains of the rats histologically to localize all recording sites. At the end of each recording session, we induced electrolytic lesions by passing currents ($3–5$ μA, 2×2 s, unipolar) through the tips of the electrodes. The brains were sectioned (coronally for cortical and thalamic recordings and parasagittally for brainstem recordings) and stained for cytochrome oxidase activity[28]. In these preparations, the different cortical layers, barrel borders, thalamic and brainstem nuclei, lesions and electrode tracks were clearly visible (Fig. 1).

Data analysis

Only data from well localized recording sites (see Fig. 1) are described. We computed PSTHs using 1-ms bins and smoothed them by convolution with a triangle of area 1 and a base of ± 8 ms. Neuronal latencies were estimated from the smoothed PSTHs as the time in which the firing rate crossed the half-peak value (after subtracting background activity). Other latency estimations, such as latency to peak or to 0.1 peak value, yielded basically the same results. Spike counts were the average sum (per stimulus cycle) of spikes during the first 100 ms after stimulus onset.

Received 28 December 1999; accepted 1 May 2000.

1. Woolsey, T. A. in *Encyclopedia of Neuroscience* (eds Adelman, G. & Smith, B.) 195–199 (Elsevier, Amsterdam, 1997).
2. Diamond, M. E. & Armstrong-James, M. Role of parallel sensory pathways and cortical columns in learning. *Concepts Neurosci.* **3,** 55–78 (1992).
3. Diamond, M. E., Armstrong-James, M. & Ebner, F. F. Somatic sensory responses in the rostral sector of the posterior group (POm) and in the ventral posterior medial nucleus (VPM) of the rat thalamus. *J. Comp. Neurol.* **318,** 462–476 (1992).
4. Diamond, M. E., Armstrong-James, M., Budway, M. J. & Ebner, F. F. Somatic sensory responses in the rostral sector of the posterior group (POm) and in the ventral posterior medial nucleus (VPM) of the rat thalamus: dependence on the barrel field cortex. *J. Comp. Neurol.* **319,** 66–84 (1992).
5. Hoogland, P. V., Welker, E., Van der Loos, H. & Wouterlood, F. G. in *Cellular Thalamic Mechanisms* (eds Bentivoglio, M. & Spreafico, R.) 152–162 (Elsevier, Amsterdam, 1988).
6. Chmielowska, J., Carvell, G. E. & Simons, D. J. Spatial organization of thalamocortical and corticothalamic projection systems in the rat SmI barrel cortex. *J. Comp. Neurol.* **285,** 325–338 (1989).
7. Lu, S. M. & Lin, R. C. Thalamic afferents of the rat barrel cortex: a light- and electron-microscopic study using *Phaseolus vulgaris* leucoagglutinin as an anterograde tracer. *Somatosens. Mot. Res.* **10,** 1–16 (1993).
8. Koralek, K. A., Jensen, K. F. & Killackey, H. P. Evidence for two complementary patterns of thalamic input to the rat somatosensory cortex. *Brain Res.* **463,** 346–351 (1988).
9. Carvell, G. E. & Simons, D. J. Biometric analyses of vibrissal tactile discrimination in the rat. *J. Neurosci.* **10,** 2638–2648 (1990).
10. Hartings, J. A. & Simons, D. J. Thalamic relay of afferent responses to 1- to 12-Hz whisker stimulation in the rat. *J. Neurophysiol.* **80,** 1016–1019 (1998).
11. Nicolelis, M. A. & Chapin, J. K. Spatiotemporal structure of somatosensory responses of many-neuron ensembles in the rat ventral posterior medial nucleus of the thalamus. *J. Neurosci.* **14,** 3511–3532 (1994).
12. Welker, W. I. Analysis of sniffing of the albino rat. *Behaviour* **22,** 223–244 (1964).
13. Fanselow, E. E. & Nicolelis, M. A. L. Behavioral modulation of tactile responses in the rat somatosensory system. *J. Neurosci.* **19,** 7603–7616 (1999).
14. Friedberg, M. H., Lee, S. M. & Ebner, F. F. Modulation of receptive field properties of thalamic somatosensory neurons by the depth of anesthesia. *J. Neurophysiol.* **81,** 2243–2252 (1999).
15. Simons, D. J., Carvell, G. E., Hershey, A. E. & Bryant, D. P. Responses of barrel cortex neurons in awake rats and effects of urethane anesthesia. *Exp. Brain Res.* **91,** 259–272 (1992).
16. Chiaia, N. L., Rhoades, R. W., Fish, S. E. & Killackey, H. P. Thalamic processing of vibrissal information in the rat: II. Morphological and functional properties of medial ventral posterior nucleus and posterior nucleus neurons. *J. Comp. Neurol.* **314,** 217–236 (1991).
17. Crabtree, J. W., Collingridge, G. L. & Isaac, J. T. A new intrathalamic pathway linking modality-related nuclei in the dorsal thalamus. *Nature Neurosci.* **1,** 389–394 (1998).
18. Ahissar, E. Temporal-code to rate-code conversion by neuronal phase-locked loops. *Neural Comput.* **10,** 597–650 (1998).
19. Kleinfeld, D., Berg, R. W. & O'Connor, S. M. Anatomical loops and their electrical dynamics in relation to whisking by rat. *Somatosens. Mot. Res.* **16,** 69–88 (1999).
20. White, E. L. & Keller, A. Intrinsic circuitry involving the local axon collaterals of corticothalamic projection cells in mouse SmI cortex. *J. Comp. Neurol.* **262,** 13–26 (1987).
21. Swadlow, H. A. Influence of VPM afferents on putative inhibitory interneurons in s1 of the awake rabbit—evidence from cross-correlation, microstimulaton, and latencies to peripheral sensory stimulation. *J. Neurophysiol.* **73,** 1584–1599 (1995).
22. Silva, L. R., Amitai, Y. & Connors, B. W. Intrinsic oscillations of neocortex generated by layer 5 pyramidal neurons. *Science* **251,** 432–435 (1991).
23. Nicolelis, M. A. L., Baccala, L. A., Lin, R. C. S. & Chapin, J. K. Sensorimotor encoding by synchronous neural ensemble activity at multiple levels of the somatosensory system. *Science* **268,** 1353–1358 (1995).
24. Ahissar, E., Haidarliu, S. & Zacksenhouse, M. Decoding temporally encoded sensory input by cortical oscillations and thalamic phase comparators. *Proc. Natl Acad. Sci. USA* **94,** 11633–11638 (1997).
25. Sherman, S. M. & Guillery, R. W. Functional organization of thalamocortical relays. *J. Neurophysiol.* **76,** 1367–1395 (1996).

26. Zucker, E. & Welker, W. I. Coding of somatic sensory input by vibrissae neurons in the rat's trigeminal ganglion. *Brain Res.* **12,** 138–156 (1969).
27. Carr, C. E. Processing of temporal information in the brain. *Annu. Rev. Neurosci.* **16,** 223–243 (1993).
28. Haidarliu, S., Sosnik, R. & Ahissar, E. Simultaneous multi-site recordings and iontophoretic drug and dye applications along the trigeminal system of anesthetized rats. *J. Neurosci. Methods* **94,** 27–40 (1999).
29. Williams, M. N., Zahm, D. S. & Jacquin, M. F. Differential foci and synaptic organization of the principal and spinal trigeminal projections to the thalamus in the rat. *Eur. J. Neurosci.* **6,** 429–453 (1994).
30. Bourassa, J., Pinault, D. & Deschenes, M. Corticothalamic projections from the cortical barrel field to the somatosensory thalamus in rats: a single-fibre study using biocytin as an anterograde tracer. *Eur. J. Neurosci.* **7,** 19–30 (1995).

Supplementary information is available on *Nature*'s World-Wide Web site (http://www.nature.com) or as paper copy from the London editorial office of *Nature*.

Acknowledgements

We thank M. Ahissar, and S. Barash for suggestions; A. Arieli, F. F. Ebner, K. O. Johnson, R. Malach and D. J. Simons for comments and discussions; M. E. Diamond for assistance during our initial thalamic recordings; and B. Schick for reviewing the manuscript. This work was supported by the US–Israel Binational Science Foundation and by the MINERVA Foundation, Germany. S.H. was supported by The Centre for Absorption of Scientists, Ministry of Absorption, Israel.

Correspondence and requests for materials should be addressed to Ehud Ahissar (e-mail: Ehud.Ahissar@weizmann.ac.il).

Presenilin is required for proper morphology and function of neurons in *C. elegans*

Nicole Wittenburg*, Stefan Eimer*, Bernard Lakowski*, Sascha Röhrig*, Claudia Rudolph† & Ralf Baumeister*

** Genzentrum, Ludwig-Maximilians-Universitaet, Feodor-Lynen-Strasse 25, D-81377 Munich, Germany*
† EleGene GmbH, Am Klopferspitz 19, D-82152 Martinsried, Germany

Mutations in the human presenilin genes cause the most frequent and aggressive forms of familial Alzheimer's disease (FAD)[1]. Here we show that in addition to its role in cell fate decisions in non-neuronal tissues[2–4], presenilin activity is required in terminally differentiated neurons *in vivo*. Mutations in the *Caenorhabditis elegans* presenilin genes *sel-12* and *hop-1* result in a defect in the temperature memory of the animals. This defect is caused by the loss of presenilin function in two cholinergic interneurons that display neurite morphology defects in presenilin mutants. The morphology and function of the affected neurons in *sel-12* mutant animals can be restored by expressing *sel-12* only in these cells. The wild-type human presenilin PS1, but not the FAD mutant PS1 A246E, can also rescue these morphological defects. As *lin-12* mutant animals display similar morphological and functional defects to presenilin mutants, we suggest that presenilins mediate their activity in postmitotic neurons by facilitating Notch signalling. These data indicate cell-autonomous and evolutionarily conserved control of neural morphology and function by presenilins.

To study the activity of presenilin genes in neurons, we focused on *C. elegans sel-12* as the detailed morphology and function of many neurons in *C. elegans* is known. Like presenilins in other species, *C. elegans* sel-12 is strongly expressed in neurons. We tested the functional integrity of the nervous system of *sel-12* mutants by looking for defects in the execution of a variety of behaviours, such as movement and response to mechanical, chemical and thermal stimuli.

We found that *sel-12* mutants display a highly penetrant defect in their ability to sense and/or memorize temperature. Wild-type *C. elegans* display strong preference for their growth temperature, and can memorize it and store the information for several hours, suggesting a neuronal plasticity[5]. This behaviour can be studied with a simple experimental model. When placed in a radial thermal gradient on the agar surface of a petri dish, wild-type animals migrate to their preferred temperature, and then move in isothermal circles (Table 1, Fig. 1a). In contrast, the *sel-12(ar131)* and *sel-12(ar131)* and *sel-12(ar171)* mutant animals have lost the ability to perform isothermal tracks. Most animals are non-responsive to the temperature gradient and moved randomly on the plate (athermotactic behaviour), and 10% of the remaining animals moved to colder temperatures than the wild-type (cryophilic behaviour). These results indicate that *sel-12* mutants may have defects in the neural circuit for thermotaxis.

The neurons necessary for thermotaxis have been studied extensively by mutational analyses and laser ablation studies[6]. Temperature input activates the two AFD sensory neurons, which synapse extensively onto the two AIY interneurons. Chemical signals from AIY and AIZ (synaptic partners that represent the four central integrating interneurons), in turn, regulate postsynaptic inter- and motor neurons that control the motor response. We carefully examined the morphology of the AFD, AIZ and AIY neurons in *sel-12* animals using green fluorescent protein (GFP) reporter constructs, and saw no obvious defects in AFD and AIZ neurons (data not shown). However, we identified defects in the morphology of AIY neurons (Table 2, Fig. 2). In wild-type animals, the processes of both AIY neurons extend anteriorly from the cell bodies along the ventral cord, run around the nerve ring and meet and terminate at the dorsal midline[7] (Fig. 2e). In adult *sel-12* mutants the AIY cell bodies are correctly positioned in the head ganglion. However, the AIY axons often grow too far anteriorly before turning and fasciculating in the nerve ring (Fig. 2d), and/or do not stop growth at the dorsal side of the nerve ring, but turn posteriorly, sometimes extending up to the midbody region (Fig. 2b–d, classified as severe defects in Table 2). In addition, short extra neurites often emerge directly from the cell soma or branch off the primary process (Fig. 2a, classified as minor defects in Table 2). The number of animals showing these types of defects in AIY morphology was higher in *sel-12(ar171)* mutants (35% defects) than in *sel-12(ar131)* mutants (20% defects; Table 2). This is consistent with the severity of these mutations and their effect on egg-laying behaviour (*ar171* carries a nonsense mutation in *sel-12* and genetically represents a null allele, and *ar131* carries a missense mutation in *sel-12*)[2]. Behavioural defects are far more penetrant than the morphological defects, indicating that *sel-12* animals may also have more subtle defects in the AIY neurons than can be visualized with GFP

Table 1 Rescue of the *sel-12* thermotaxis defect

Genotype	Transgene	Fraction showing isothermal tracks
Wild type*		41/46
sel-12(ar131)		1/42
sel-12(ar171)		3/38
hop-1(lg1501)		0/44
lin-12(n941)		0/15
hop-1(lg1501);sel-12(ar131)		0/31
hop-1(lg1501);sel-12(ar171)		0/33
sel-12(ar171);byIs101	*sel-12::sel-12*	38/49
sel-12(ar171);byIs100	*sel-12::sel-12*	19/41
Wild type†		49/55
sel-12(ar131)†		3/40
sel-12(ar171)†		2/39
sel-12(ar131); byEx103†	*ttx-3::sel-12*	18/42
sel-12(ar131); byEx115†	*ttx-3::sel-12*	21/41
sel-12(ar131); byEx115†	*ttx-3::sel-12*	35/67
sel-12(ar171); byEx115†	*ttx-3::sel-12*	18/41

* Strain carries a *daf-6(e1377)* mutation that did not affect thermotaxis behaviour.
† Animals expressing *ttx-3::GFP*.
byIs100 and *byIs101* are independent chromosomally integrated arrays expressing *sel-12* cDNA from the *sel-12* promoter.

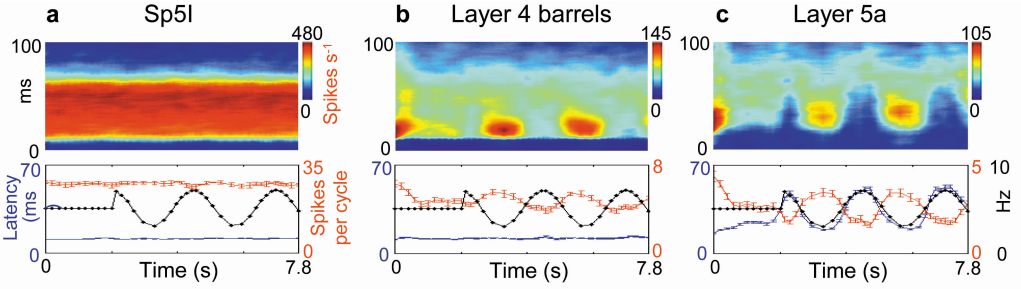
a
Sp5I
480
100
ms
Spikes s-1
0
0
b
Layer 4 barrels
145
100
0
0
c
Layer 5a
105
100
0
0
70
Latency (ms
0
35
Spikes per cycle
0
Time (s)
7.8
70
0
8
0
Time (s)
7.8
70
0
5
0
10
Hz
0
Time (s)
7.8